



A soft-chemistry route to prepare halide perovskite nanocrystals with tunable emission and high optical performance

Thais C. A. da Silva ¹ · Carolina Fernández-Saiz ^{1,3} · Rafael S. Sánchez ¹ · Andrés F. Gualdrón-Reyes ^{1,2} · Iván Mora-Seró ¹ · Beatriz Julián-López ¹

Received: 30 January 2023 / Accepted: 13 June 2023
© The Author(s) 2023

Abstract

Cesium lead halide perovskites constitute a benchmark family of inorganic perovskites for high performance optoelectronic devices. Hot injection is by far the most extended procedure to fabricate CsPbX₃ (X: Cl, Br, and/or I) perovskite nanocrystals (PNCs) of high quality. However, the tedious N₂-vacuum cycles and fast heating/cooling steps hinder the large-scale production of these materials. This work presents a fast one-step methodology to fabricate small CsPb(Cl_xBr_{1-x})₃ nanocrystals with good control of the particle size and shape by using a Soft Chemistry strategy (ligand-mediated controlled growth) and microwave heating. We demonstrate that the procedure can be extended to different mixed halide perovskites, thus providing a fine tuning of the chemical composition and consequently, tunable photoluminescence (PL) emission from 522 nm for pure CsPbBr₃ to 477 nm for CsPb(Cl_{0.4}Br_{0.6})₃, high photoluminescence quantum yield (PLQY) up to ~86% (for CsPbBr₃) and narrow PL full width at half maximum ~18–26 nm. In addition, the protocol was designed in such a way that the chemistry involved in the crystal nucleation and growth of perovskites is as close as possible to that of the hot injection process, which is mechanistically well-understood, to facilitate their adoption by the perovskite research community.

Graphical Abstract

This manuscript reports a sustainable soft-chemistry route using microwave heating to prepare CsPbX₃ (X:Cl,Br) perovskite nanocrystals with tunable PL emission. Nanocrystals with excellent photoluminescence quantum yields (PLQY, up to 86%), narrow PL FWHM 18–25 nm, defined orthorhombic crystalline phase and average particle size ranging from 15 nm to 25 nm were obtained. This is a promising strategy to reach high quality luminescent NPs, opening the door to prepare low-cost and fast luminescent perovskites for optoelectronics.

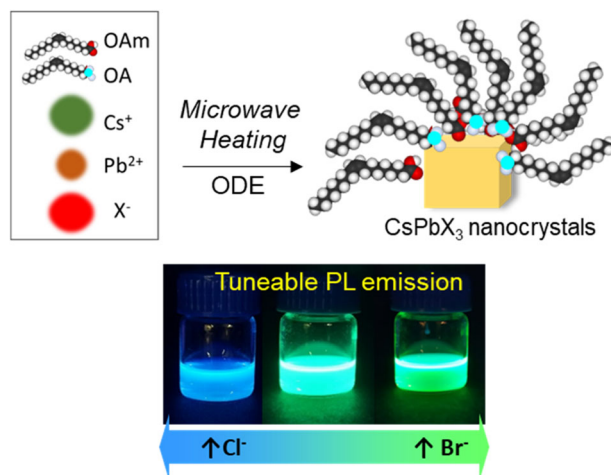
These authors contributed equally: Thais C. A. da Silva, Carolina Fernández-Saiz

✉ Beatriz Julián-López
julian@uji.es

¹ Institute of Advanced Materials (INAM), Universitat Jaume I (UJI), Avenida de Vicent Sos Baynat, s/n, 12071 Castelló de la Plana, Castelló, Spain

² Facultad de Ciencias, Instituto de Ciencias Químicas, Isla Teja, Universidad Austral de Chile, 5090000 Valdivia, Chile

³ Present address: Department of Applied Physics and Electromagnetism, University of Valencia, 46100 Valencia, Spain



Keywords Perovskite nanocrystals · Emission tuning by halide composition · Soft-chemistry · Microwave synthesis · Optoelectronics

Highlights

- Sol-gel mediated synthesis of photoluminescent CsPbX_3 ($X = \text{Br}, \text{Cl/Br}$) perovskite nanocrystals.
- Cesium carbonate and a mixture of lead halides ($\text{PbBr}_2/\text{PbCl}_2$) lead to high-quality CsPbX_3 nanocrystals via one-step fast microwave heating.
- OA, OLA, TOPO and TOP as ligands to control the nucleation and growth of oleylammonium-oleate capped PNCs.
- Facile tuneability of the absorption and emission properties through PbCl_2 addition.

1 Introduction

Metal halide perovskite nanocrystals (PNCs) have consolidated as prominent luminescent semiconductors due to their outstanding intrinsic properties and potential applications in optoelectronics [1], photovoltaics [2], solar-driven photo(electro)chemistry [3], and photonics [4] among others. Interesting features such as low-cost and facile preparation [5], modulable band gap covering the UV–vis–NIR spectrum (making use of quantum confinement regime or composition tunability) [6–8], narrow full-width at half-maximum (FWHM) photoluminescence (PL) emission and enhanced radiative recombination dynamics [8], have been well exploited to fabricate multicolor light emitting diodes [9] and PNCs-based solar cells [10] with breakthroughs in the current state-of-the-art. Among the metal halide perovskites, pure inorganic CsPbBr_3 exhibits the best compromise between optoelectronic features (excellent photoluminescence quantum yield (PLQY) and narrow FWHM) and high chemical stability required to prepare active layers based on high-quality PNCs with low density of structural defects.

Accordingly, several synthetic routes have been reported to modify the main parameters such as temperature, time of reaction, and stoichiometry of initial precursors and thereby

obtain less-defective nanoparticles (NPs) [11–13]. Among the most well-known methodologies, the hot-injection approach has been widely reported to produce PNCs in a broad range of temperatures (140–260 °C) [5, 14], favor their composition engineering and achieve more homogeneous nanocrystal particle sizes. Nevertheless, this procedure involves the use of vacuum and inert atmospheres for long times and requires a more complex experimental setup. This fact makes difficult their scaling up for future technologies. To overcome this issue, more flexible and profitable procedures such as the solvothermal method have been attractive for the preparation of nanomaterials [15, 16], where the initial precursors are combined into a pressurized autoclave under an isochoric environment at high temperatures. In this line, the morphology, crystalline structure, and size monodispersity of the final PNCs can be controlled; unfortunately, this route requires long reaction times (≥ 1 h) with a high energy demand [17]. Therefore, optimized alternatives such as chemical vapor deposition, have also been used for the growth of high-quality perovskites [18], but the harsh synthesis parameters and the limited capability to modulate the morphology restrict the growth of nanoscale systems with diverse morphologies.

Unlike the abovementioned synthetic routes, the microwave (MW)-assisted method has emerged as one of the

most flexible, sustainable and facile strategies to promote the growth of CsPbX_3 (X: Cl, Br, I) PNCs with improved photophysical features, where high-frequency irradiation is essential to conduct chemical reactions [17, 19, 20]. Compared to the conductive/convective energy transfer induced by increasing the synthesis temperature, microwave radiation produces a more homogeneous heating within the whole volume of the polar mixture reaction, hence promoting the formation of uniform nucleation sites [21, 22]. At this point, better monodispersity in PNCs is achieved, reducing the reaction time [17]. The limited literature on the use of MW to synthesize CsPbBr_3 PNCs reports the use of cesium acetate (CsOAc) instead of cesium carbonate (Cs_2CO_3) since the former precursor shows better solubility within the mixture reaction [19, 20]. However, for the synthesis of the ionic CsPbBr_3 , the highest optical performance obtained for PNCs by hot injection have been reached by using Cs_2CO_3 , which suggest the formation of nanoparticles (NPs) with lower content of crystalline defects. In the MW-assisted synthesis, the presence of carbonate, as a divalent anion, can significantly influence the capability of the reaction medium to convert radiation into heat, differing from the previous works using the microwave approach, in which a less polar acetate reagent was used.

Herein, we have developed a fast and easy one-step microwave-assisted synthesis of CsPbX_3 nanocrystals with excellent optoelectronic properties using appropriate reagents (cesium carbonate and lead halides) and avoiding the use of tedious N_2 -vacuum cycles of hot injection synthesis. We demonstrate that the route is versatile and different $\text{CsPb}(\text{Cl}_x\text{Br}_{1-x})_3$ PNCs (x ranging from 0 to 0.75) with tunable PL emission can be obtained by varying the Cl/Br composition through varying the ratio of lead halides ($\text{PbBr}_2/\text{PbCl}_2$). The resulting NPs show high PLQY up to ~86%, narrow PL FWHM ~18–26 nm, defined orthorhombic crystalline phase and average particle size ranging from ~15 nm to ~25 nm. The introduction of the small halide (Cl) induces a decrease in the particle size distribution of PNCs, and monodispersity is maintained. Therefore, we propose this synthetic approach as a promising and up-scalable strategy to reach high quality NPs with high PL properties, thus opening the door for a technological deployment of luminescent perovskites for optoelectronics.

2 Experimental section

2.1 Reagents

Cesium carbonate (Cs_2CO_3 , 99.9%), oleic acid (OA, 90%), oleylamine (OLA, 80–90%) and trioctylphosphine oxide (TOPO, 99%) were purchased from Sigma-Aldrich. Lead

halide (PbX_2 , X = Cl, Br, ultradry 99.999%) was purchased from ABCR. Trioctylphosphine (TOP, 97%) and 1-octadecene (ODE, tech. 90%) were purchased from Alfa Aesar. Hexane (97%) and MeOAc were purchased from ACROS organics. OA and OLA were degassed for 1 h under vacuum at 110 °C before the synthesis, and the solutions were stocked in the fridge. Other chemicals were used as received without any further purification.

2.2 Preparation of CsPbX_3 Perovskite NCs

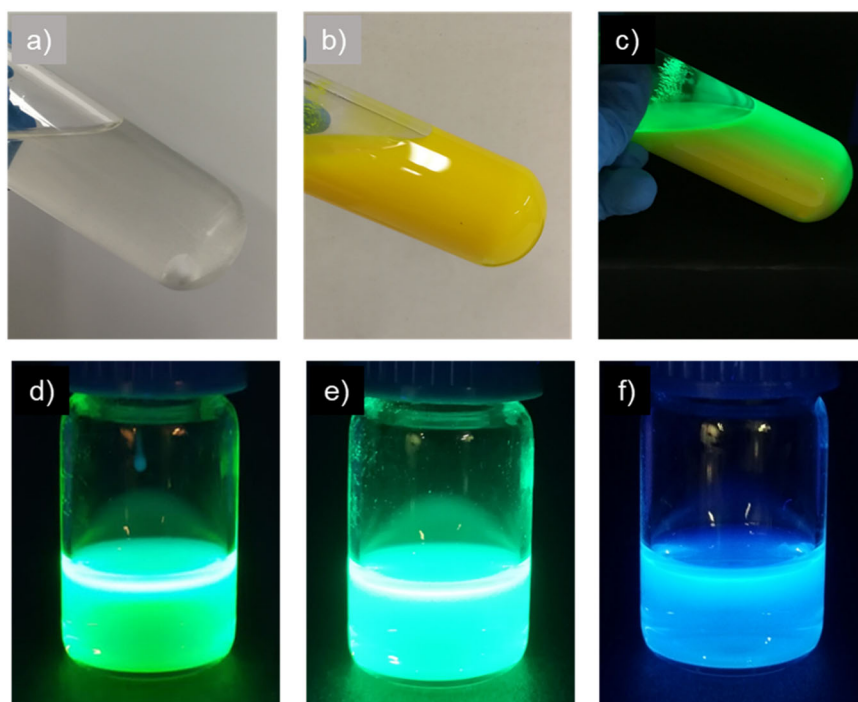
The synthesis of three perovskites with different chloride-to-bromide ratio was developed in this work: CsPbBr_3 , $\text{CsPb}(\text{Cl}_{0.25}\text{Br}_{0.75})_3$ and $\text{CsPb}(\text{Cl}_{0.4}\text{Br}_{0.6})_3$. These stoichiometries were selected from the literature (from hot injection methodology) to achieve nanocrystals with tunable bandgap and different optoelectronic properties. In a typical synthesis, 0.5 g of TOPO were loaded into a microwave tube (total volume of 30 mL). Then, 15 mL of ODE, 1 ml OA and 1 ml OLA were added and stirred at 50 °C until complete dissolution, giving a pale yellowish solution. Hereafter, Cs_2CO_3 (0.0988 mmol) and PbBr_2 (0.35 mmol) were added in the reaction tube. After 5 min of stirring, see Fig. 1a, the tube was placed in the MW reactor and heated at ~80 °C min^{-1} up to 160 °C for 5 min (variable power from 0 to 850 W to reach the desired temperature). During the reaction, a color change of the reaction mixture was clearly seen (see video in the Supporting Information), indicating the formation of the PNCs, see Fig. 1b. The system was cooled down with compressed air for ~1 min. Figure 1c shows the typical green luminescence of the CsPbBr_3 colloidal crude product upon excitation with a UV lamp at 365 nm. The yellowish dispersion was precipitated with MeOAc (5 mL), and the PNC product was extracted from the crude solution by centrifuging at 10000 rpm for 5 min. After discarding the supernatant, the solid was further purified by redispersing in hexane (5 mL), then adding MeOAc (5 mL) and centrifuged at 5000 rpm for 5 min to recover the PNCs; this washing cycle was performed twice to ensure a suitable degree of purity. Finally, the nanocrystals were redispersed in hexane (2 mL) for further characterization.

The mixed halide $\text{CsPb}(\text{Cl}_{0.25}\text{Br}_{0.75})_3$ and $\text{CsPb}(\text{Cl}_{0.4}\text{Br}_{0.6})_3$ NCs were similarly prepared, but PbBr_2 was replaced by the appropriated mixture of PbBr_2 and PbCl_2 salts (0.263 mmol PbBr_2 + 0.087 mmol PbCl_2 ; 0.210 mmol PbBr_2 + 0.140 mmol PbCl_2 , respectively), and 2 ml of TOP were also added in the reaction mixture to facilitate the solubility of the chloride salt. The final aspect of the three as-synthesized PNCs dispersions in hexane is shown in Fig. 1d–f.

2.3 Instrumental techniques

The microwave heating was performed on the monomode microwave reactor model Monowave 400 from Anton Paar.

Fig. 1 Images of the reaction mixture for CsPbBr_3 sample **a** before MW heating, **b** after MW heating, **c** after MW heating upon 365 nm excitation. Photographs of the final suspensions of PNCs in hexane of **d** CsPbBr_3 , **e** $\text{CsPb}(\text{Cl}_{0.25}\text{Br}_{0.75})_3$ and **f** $\text{CsPb}(\text{Cl}_{0.4}\text{Br}_{0.6})_3$ upon 365 nm excitation



The vial (reactor) was made of borosilicate glass, with a filling volume between 6 mL and 30 mL. This equipment is designed for small- to medium-scale microwave synthesis, and allows consumable costs to be reduced, by using reusable vials, caps, and septa, thus contributing to a reduced environmental footprint. X-ray diffraction (XRD) of the perovskite crystals was undertaken on a D4 Endeavor diffractometer from Bruker-AXS, with a Bragg-Brentano ($\theta/2\theta$) geometry and $\text{Cu K}\alpha$ radiation ($\lambda = 0.15406$ nm). The data were collected from 15° to 60° with a step scan of 0.05° and 1.5 s/step of counting time. The morphology of the samples was analyzed with a JEOL JEM-3100 field emission scanning electron microscope equipped with an energy dispersive spectroscopy system INCA 250 (Oxford) using an acceleration voltage of 20 kV. For the sample preparation, the nanocrystals were dried with a nitrogen flow and the powders were directly deposited on a carbon film and coated with Au-Pt. Transmission electron microscopy (TEM) images were registered with a JEOL- 2100 LaB₆ microscope, operating at an accelerating voltage of 200 kV, and coupled to an Inca Energy TEM 200 (Oxford) energy dispersive x-ray spectrometer. The suspension of nanocrystals in hexane was directly deposited onto carbon-coated copper grids. A spectrophotometer Lambda 1050 + UV/Vis/NIR (from PerkinElmer) was used for the UV-VIS-NIR absorption measurements. For the analysis, the samples were measured from 1200 nm to 350 nm with spectral resolution of 2 nm. The emission and excitation spectra were measured on a Cary ECLIPSE fluorescence spectrophotometer (Varian) in quartz cuvettes with 5 nm slit

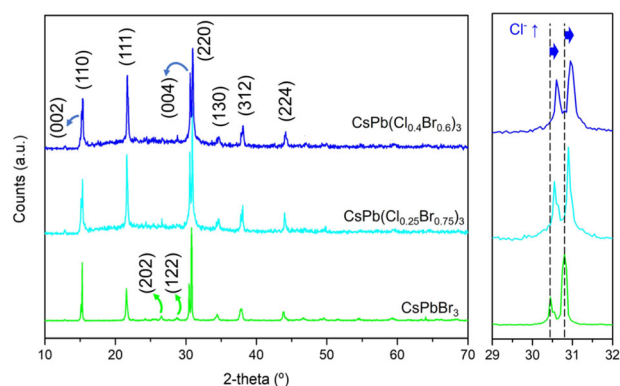


Fig. 2 Left: XRD patterns of the synthesized $\text{CsPb}(\text{Cl}_x\text{Br}_{1-x})_3$ PNCs. Planes associated with the orthorhombic CsPbBr_3 phase (ICSD 97851). Right: inset of the region $29\text{--}32^\circ$ 2-theta showing the shift of the 004 and 220 planes towards higher angles with chlorine incorporation

and medium scan rate. PLQY measurements were carried out using an absolute quantum yield spectrometer (C9920-02, Hamamatsu) with an excitation of 390 nm.

3 Results and discussion

The XRD patterns of the as-synthesized PNCs with different Cl/Br molar ratio are shown in Fig. 2. The experimental patterns reveal the formation of the orthorhombic CsPbBr_3 structure with $Pbnm$ space group for all samples, as a single phase, corresponding to the ICSD 97851 card. This crystalline

Fig. 3 **a** SEM and **b** TEM and images of the synthesized CsPbBr_3 PNCs. Inset of Fig. 3b exhibits the HRTEM of the nanocrystals sample

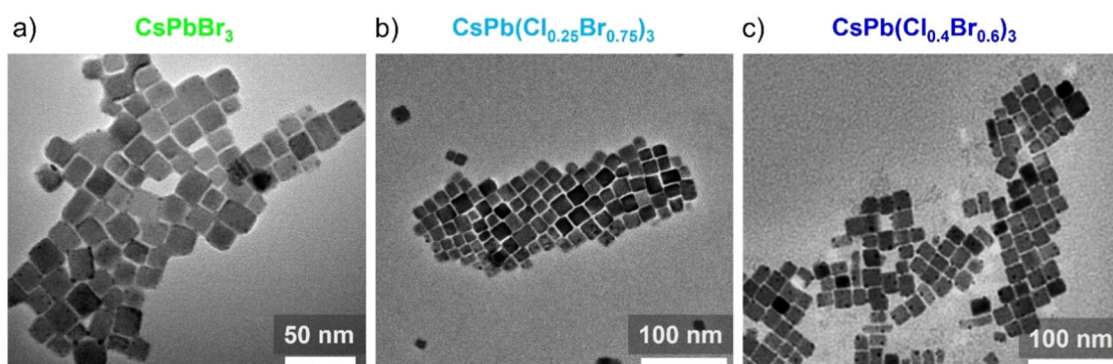
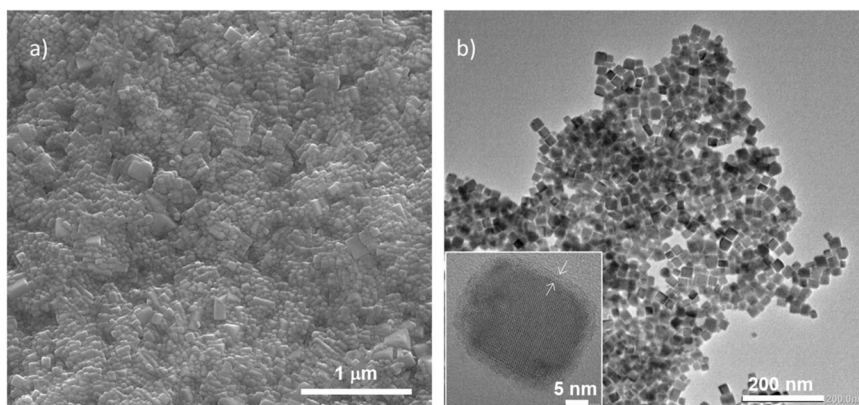


Fig. 4 Typical TEM micrographs of as-synthesized PNCs with the compositions: **(a)** CsPbBr_3 , **(b)** $\text{CsPb}(\text{Cl}_{0.25}\text{Br}_{0.75})_3$ and **(c)** $\text{CsPb}(\text{Cl}_{0.4}\text{Br}_{0.6})_3$

phase is preferred by the system when perovskite nucleation occurs at relatively low temperature [23], differing from nanocrystals prepared by hot injection, in which the cubic phase is usually obtained [5]. In our procedure, the orthorhombic crystallization can be attributed to a combined effect of a faster heating process and lower synthesis temperature. Interestingly, both structures have direct energy bandgap and possess similar optical properties [24], despite the variations in their lattice constants. When increasing chloride in the stoichiometry, the XRD peaks shift towards higher 2θ angles (Fig. 2 right panel), up to 0.24° 2 -theta, indicating the compression of the perovskite lattice attributed to the reduction of the Pb-X bonds by decreasing the ionic radius of halide during bromide-to-chloride substitution ($r(\text{Br}^-)$: 1.95 Å and $r(\text{Cl}^-)$: 1.81 Å). The Scherrer equation [24] was used to determine the average crystallite size of the crystalline domains, giving values of 28 nm, 21 nm, and 16 nm for CsPbBr_3 , $\text{CsPb}(\text{Cl}_{0.25}\text{Br}_{0.75})_3$ and $\text{CsPb}(\text{Cl}_{0.4}\text{Br}_{0.6})_3$ samples, respectively. The average crystallite size reduces as the chloride ion content is increasing in the structure.

The morphology of the samples was analyzed by SEM and TEM. Figure 3a shows a representative SEM micrograph of the CsPbBr_3 dried powders composed of cubic shaped nanoparticles of an average edge length of 25 nm (calculated from averaging the size of 150 nanocubes), although some

polydispersity in the crystal size is detected. Figure 3b shows a TEM micrograph, confirming not only the cubic morphology but also the crystallinity of the synthesized nanocrystals. Indeed, the inset of Fig. 3b shows the crystalline plane of the orthorhombic structure, and Fig. S1 includes a selected area electron diffraction pattern and the hkl associated rings. An organic shell of ~ 1.5 nm around the nanocrystals is clearly observed in the inset of Fig. 3b, attributed to the presence of remaining oleic species from the synthesis helping to stabilize the nanocrystals in hexane suspension and avoiding perovskite degradation by moisture. EDS analyses give atomic percentages in good agreement with the theoretical CsPbBr_3 stoichiometry (Fig. S2). Then, the high thermal stability of capping ligands at the reaction temperature (160°C) allows a good control of the nanocrystal size. If the reaction mixture is heated sufficiently to compromise the thermal stability of the ligands [7], the crystal growth is not properly limited and polydisperse bigger particles are obtained (Fig. S3).

The effect of mixing chloride and bromide anions in the reaction induces some differences in the crystal formation (Fig. 4). All samples exhibited cubic shape, but CsPbBr_3 NPs presented larger sizes than those including chloride in their composition. The increasing amount of chloride induces a decrease in the particle size, from average 25 nm-size cubes for pure bromide to 15 nm cubes for $\text{CsPb}(\text{Cl}_{0.4}\text{Br}_{0.6})_3$ (value

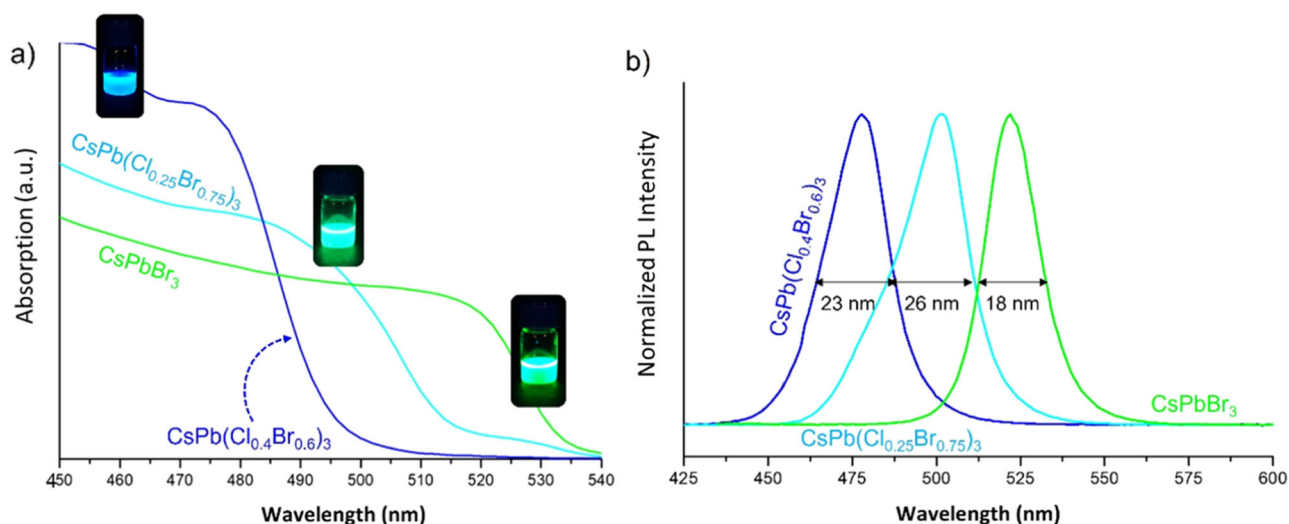


Fig. 5 **a** UV–vis absorption and **b** corresponding PL spectra of $\text{CsPb}(\text{Cl}_x\text{Br}_{1-x})_3$ PNCs. Insets of Fig. 5a show the nanocrystal suspensions under UV excitation lamp (365 nm)

Table 1 Absorption and PL properties of the $\text{CsPb}(\text{Cl}_x\text{Br}_{1-x})_3$ PNCs synthesized by microwave method

Perovskite material	Absorption band gap (nm)	PL emission peak position (nm)	Full Width at Half Maximum (nm)	PLQY (%)
$\text{CsPb}(\text{Cl}_{0.4}\text{Br}_{0.6})_3$	476.8	477.2	23.3	51
$\text{CsPb}(\text{Cl}_{0.25}\text{Br}_{0.75})_3$	501.9	501.7	26.1	67
CsPbBr_3	523.1	522.8	18.5	86

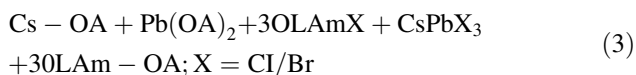
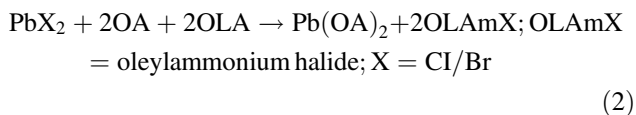
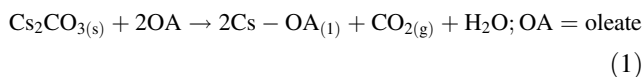
of maximum average particle size distribution). This result is in good agreement with XRD measurements, as the introduction of a higher content of smaller chloride anions not only favors the compression of the nanocrystal lattice, but also a decrease in particle size [25]. Compositional analyses performed by EDS provided atomic percentages which are also in good agreement with the theoretical formula of the mixed chloride-bromide perovskites (Fig. S4). This means that the amount of halide in the synthesized perovskite nanocrystals can be easily modulated by using a suitable stoichiometry of the respective PbX_2 precursors.

The UV–vis absorption spectra of the samples are displayed in Fig. 5a, where an intense absorption onset located in the visible region is associated with the direct band gap of the semiconductor CsPbX_3 nanocrystals. A blueshift in this optical feature is achieved with increasing chloride ions in the perovskite. The optical band gaps were determined from Tauc plot graphs (Fig. S5), ranging from 2.60 eV (476.8 nm), 2.47 eV (501.9 nm), and 2.37 (523.1 nm) for $\text{CsPb}(\text{Cl}_{0.4}\text{Br}_{0.6})_3$, $\text{CsPb}(\text{Cl}_{0.25}\text{Br}_{0.75})_3$, and CsPbBr_3 PNCs, respectively. This result perfectly agrees with the results reported in the literature for these compositions [6]. On the other hand, the PL spectra of the three samples are represented in Fig. 5b. According to the variation of the absorption onset, the PL emission peak position was also displaced with the halide composition, ranging from 522.8 nm for CsPbBr_3 to

477.2 nm for $\text{CsPb}(\text{Cl}_{0.4}\text{Br}_{0.6})_3$. A minor enlargement of the full-width at half-maximum (FWHM) after chlorine incorporation is observed, due to a lattice distortion by Cl incorporation [25]. These results reveal that the absorption and emission properties of the perovskites can be easily tuned by simply adjusting the halide composition in the reaction. The inset of Fig. 5b shows the typical blue and green emission observed by the naked eye of the synthesized PNCs suspensions. By increasing the amount of PbCl_2 added to the mixture reaction, more Pb–Cl bonds are generated within the material structure, providing the halide positions. Considering the smaller ionic radius of Cl^- compared to that of Br^- species, a shrinking of the $[\text{PbX}_6]$ octahedra in the mixed halide $\text{CsPb}(\text{Cl}_x\text{Br}_{1-x})_3$ lattice is favored, promoting the increase in the band gap, which is reflected in a blue-shifted PL. This result agrees with the displacement of the XRD peaks to higher Bragg angles, as a consequence of the lattice contraction. In addition, the PLQY of samples was estimated, giving values around 51%, 67%, and 86% for $\text{CsPb}(\text{Cl}_{0.4}\text{Br}_{0.6})_3$, $\text{CsPb}(\text{Cl}_{0.25}\text{Br}_{0.75})_3$, and CsPbBr_3 PNCs, respectively. This trend infers that the presence of a higher content of Br^- domains favors the decrease of deep states formed by chloride species, promoting the improvement of radiative recombination [26]. Absorption and PL features of the $\text{CsPb}(\text{Cl}_x\text{Br}_{1-x})_3$ NCs by varying the Cl content are summarized in Table 1.

To check the optical performance of our materials, we compared them with the optical features of the pioneering work of Kovalenko in which 4–15 nm CsPbX₃ NCs with cubic shape were prepared by hot injection [5]. The absorption band gaps and maximum emission peaks present a good match with similar compositional bandgap engineering. The photoluminescence of Kovalenko's CsPbX₃ NCs are characterized by narrow emission line widths of 12–42 nm and high quantum yields of 50–90%. Our values are completely in agreement with those obtained by hot injection. Hence, our materials exhibit comparable optical features compared to those of the hot injection method through a much faster and easy route.

To provide a mechanism for the formation of CsPbX₃ PNCs using the MW approach, it is pivotal to depict the chemical reactions taking place in the presence of capping ligands such as oleic acid (OA) and oleylamine (OLA): [14]



As a first step in the CsPbX₃ growth, OA can react with Cs₂CO₃ during the microwave heating to generate Cs-oleate (1). However, considering that the amounts of OA and OLA are stoichiometric to promote the dissolution of the halide precursor, TOPO is added to facilitate the Cs₂CO₃ dissolution. By reacting PbX₂ (X = Br and Cl/Br combinations) with OA and OLA, Pb-oleate (Pb-OAc) and oleylammonium halide (OLAmX) are produced (2). At this stage, OLAmX is intercalated into the [PbX₆] octahedra building blocks to generate a corner-sharing structure. Lastly, Cs⁺, Pb-OA and OLAmX react in the reaction mixture to form CsPbX₃ and oleylammonium oleate (OLAm-OA) (3), which is the main ligand to mediate the stabilization of the perovskite product. These reactions are much facilitated by the fast heating of the microwave radiation. Despite the minimal capacity of the nonpolar solvent (ODE) to convert microwave energy into heat (tan δ < 0) [27], the presence of polar reagents dispersed in the reaction mixture such as Cs⁺ and Pb²⁺ metal salts, halide anions, and especially carbonate species, significantly increases the heating rate. In addition, the formation of the first nuclei of PNCs, which are highly ionic species, also enhances the microwave absorption properties of the reaction mixture. Thus, even if our work has been performed in a laboratory microwave reactor limited to reaction volumes of a

few milliliters, the polar nature of the media promotes significant power absorption and conversion to heat in large volumes. Therefore, we envisage this route as a very promising approach for the technological applications of PNCs in which scale up is a requirement.

4 Conclusions

In this work, we have implemented a soft chemistry route to prepare highly luminescent CsPb(Cl_xBr_{1-x})₃ PNCs with tunable PL properties. By introducing stoichiometric quantities of the corresponding PbCl₂ and PbBr₂ precursors, nanocrystal suspensions were prepared with excellent monodispersity with a tunable PL emission from 522 nm for green-emitting CsPbBr₃ to 477 nm for blue-emitting CsPb(Cl_{0.4}Br_{0.6})₃, taking advantage of the homogeneous nucleation and growth provided by the microwave heating. In this way, a narrow FWHM between 18–26 nm was obtained, yielding an improved optical performance deduced from PLQY values of 51%, 67%, and 86%, by increasing the Br content into the nanocrystals. This fact implies that the introduction of a higher density of Br domains decreases the deep energy states promoted by the presence of chloride species within the perovskite structure, increasing the radiative carrier recombination rate. This synthetic route offers a fast, simple and low-cost strategy to obtain mixed halide PNCs with promising photophysical features to be applied in optoelectronic devices.

Author contributions All authors contributed to the study conception and design. Material synthesis, characterization and data collection were mainly performed by TCAdS and CF-S. RSS, IM-S, AFG-R and BJ-L participated in the data analysis and results discussion. The first draft of the manuscript was written by AFG-R and BJ-L, with the contribution of TCAdS and CF-S in the figures. AFG-R designed the image for the cover of the issue. All authors read and approved the final manuscript.

Funding This work is a result of the project STABLE PID2019-107314RB-I00 funded by MCIN/AEI/10.13039/501100011033/ and PROMETEO Program from Generalitat Valenciana (reference CIPROM/2021/078). BJL, TCS, and CF-S acknowledge the financial support from Universitat Jaume I (project UJI-B2021-50). TCS would like to thank Generalitat Valenciana for her Ph.D. contract (GRISO-LIAP/2021/096). Open Access funding provided thanks to the CRUE-CSIC agreement with Springer Nature.

Compliance with ethical standards

Conflict of interest The authors declare no competing interests.

Publisher's note Springer Nature remains neutral with regard to jurisdictional claims in published maps and institutional affiliations.

Supplementary information The online version contains supplementary material available at <https://doi.org/10.1007/s10971-023-06171-1>.

Open Access This article is licensed under a Creative Commons Attribution 4.0 International License, which permits use, sharing, adaptation, distribution and reproduction in any medium or format, as long as you give appropriate credit to the original author(s) and the source, provide a link to the Creative Commons license, and indicate if changes were made. The images or other third party material in this article are included in the article's Creative Commons license, unless indicated otherwise in a credit line to the material. If material is not included in the article's Creative Commons license and your intended use is not permitted by statutory regulation or exceeds the permitted use, you will need to obtain permission directly from the copyright holder. To view a copy of this license, visit <http://creativecommons.org/licenses/by/4.0/>.

References

- Kim Y-H, Kim S, Kakekhani A, Park J, Park J, Lee Y-H, Xu H, Nagane S, Wexler RB, Kim D-H, Jo SH, Martínez-Sarti L, Tan P, Sadhanala A, Park G-S, Kim Y-W, Hu B, Bolink HJ, Yoo S, Friend RH, Rappe AM, Lee T-W (2021) *Nat Photonics* 15:148
- Sanehira EM, Marshall AR, Christians JA, Harvey SP, Ciesielski PN, Wheeler LM, Schulz P, Lin LY, Beard MC, Luther JM (2017) *Sci Adv* 3:eaa04204
- Fernández-Climent R, Gualdrón-Reyes AF, García-Tecedor M, Mesa CA, Cárdenas-Morcoso D, Montañes L, Barea EM, Mas-Marzá E, Julián-López B, Mora-Seró I, Giménez S (2021) *Solar RRL* 6:2100723
- Suárez I, Juárez-Pérez EJ, Bisquert J, Mora-Seró I, Martínez-Pastor JP (2015) *Adv Mater* 27:6157
- Protesescu L, Yakunin S, Bodnarchuk MI, Krieg F, Caputo R, Hendon CH, Yang RX, Walsh A, Kovalenko MV (2015) *Nano Lett* 15:3692
- Nedelcu G, Protesescu L, Yakunin S, Bodnarchuk MI, Grotevent MJ, Kovalenko MV (2015) *Nano Lett* 15:5635
- Hassanabadi E, Latifi M, Gualdrón-Reyes AF, Masi S, Y. joon S, Poyatos M, Julián-López B, Mora Seró I (2020) *Nanoscale* 12:14194
- Protesescu L, Yakunin S, Kumar S, Bär J, Bertolotti F, Masciocchi N, Guagliardi A, Grotevent M, Shorubalko I, Bodnarchuk MI, Shih C-J, Kovalenko MV (2017) *ACS Nano* 11:3119
- Kim JS, Heo J-M, Park G-S, Woo S-J, Cho C, Yun HJ, Kim D-H, Park J, Lee S-C, Park S-H, Yoon E, Greenham NC, Lee T-W (2022) *Nature* 611:688
- Hao M, Bai Y, Zeiske S, Ren L, Liu J, Yuan Y, Zarrabi N, Cheng N, Ghasemi M, Chen P, Lyu M, He D, Yun J-H, Du Y, Wang Y, Ding S, Armin A, Meredith P, Liu G, Cheng H-M, Wang L (2020) *Nat Energy* 5:79
- Guhrenz C, Benad A, Ziegler C, Haubold D, Gaponik N, Eychmüller A (2016) *Chem Mater* 28:9033
- Grisorio R, Fanizza E, Allegretta I, Altamura D, Striccoli M, Terzano R, Giannini C, Vergaro V, Ciccarella G, Margiotta N, Suranna GP (2020) *Nanoscale* 12:623
- Pradhan N (2022) *ACS Phys Chem Au* 2:268
- Zhang Y, Siegler TD, Thomas CJ, Abney MK, Shah T, De Gorostiza A, Greene RM, Korgel BA (2020) *Chem Mater* 32:5410
- Chen M, Zou Y, Wu L, Pan Q, Yang D, Hu T, Tan Y, Zhong Q, Xu Y, Liu H, Sun B, Zhang Q (2017) *Adv Funct Mater* 27:1701121
- Zhai W, Lin J, Li Q, Zheng K, Huang Y, Yao Y, He X, Li L, Yu C, Liu C, Fang Y, Liu Z, Tang C (2018) *Chem Mater* 30:3714
- Thesika K, Vadivel Murugan A (2020) *Inorg Chem* 59:6161
- Wang Y, Sun X, Shivanna R, Yang Y, Chen Z, Guo Y, Wang G-C, Wertz E, Deschler F, Cai Z, Zhou H, Lu T-M, Shi J (2016) *Nano Lett* 16:7974
- Liu H, Wu Z, Gao H, Shao J, Zou H, Yao D, Liu Y, Zhang H, Yang B (2017) *ACS Appl Mater Interfaces* 9:42919
- Pan Q, Hu H, Zou Y, Chen M, Wu L, Yang D, Yuan X, Fan J, Sun B, Zhang Q (2017) *J Mater Chem C* 5:10947
- Li Y, Huang H, Xiong Y, Kershaw SV, Rogach AL (2018) *Angew Chem* 130:5935
- He Y, Zhong Y, Peng F, Wei X, Su Y, Lu Y, Su S, Gu W, Liao L, Lee S-T (2011) *J Am Chem Soc* 133:14192
- Stoumpos CC, Malliakas CD, Peters JA, Liu Z, Sebastian M, Im J, Chasapis TC, Wibowo AC, Chung DY, Freeman AJ, Wessels BW, Kanatzidis MG (2013) *Cryst Growth Des* 13:2722
- Scherrer P (1918) *Göttinger Nachrichten Math Phys* 2:98
- Ghaithan HM, Alahmed ZA, Qaid SMH, Hezam M, Aldwayyan AS (2020) *ACS Omega* 5:7468
- Lee C, Shin Y, Villanueva-Antoli A, Das Adhikari S, Rodríguez-Pereira J, Macak JM, Mesa C, Yoon SJ, Gualdrón-Reyes AF, Mora-Seró I (2021) *Chem Mater* 22:8745
- Crossley J (1973) *J Chem Phys* 58:5315